PERGAMON

International Journal of Heat and Mass Transfer 43 (2000) 1947–1963

International Journal of HEAT and MASS TRANSFER

www.elsevier.com/locate/ijhmt

Parametric study of mixed convection in channels with concave and convex surfaces

F. Moukalled[a], A. Doughan[a], S. Acharya[b,*]

[a]*Department of Mechanical Engineering, American University of Beirut, Beirut, Lebanon*
[b]*Mechanical Engineering Department, Louisiana State University, Baton Rouge, LA 70803, USA*

Received 30 July 1998; received in revised form 27 August 1999

Abstract

Mixed convection heat transfer in channels with a heated curved surface bounded by a vertical adiabatic wall has been studied numerically. Two cases are considered: in the first case, the flow experiences a convex curvature and an increasing cross-sectional flow area (adverse pressure gradient), while in the second case, the flow experiences a concave curvature with a decreasing flow cross-section (favorable pressure gradient). Results are obtained for various curvature ratios (R/L) of the concave/convex wall, and compared with straight channels of equal heated lengths and equal heights. For channels with a convex heated surface, where the increase in flow cross-sectional area decelerates the flow while buoyancy accelerates the flow, separation is observed near the heated surface at low values of Gr/Re^2 and on the opposite vertical wall at high values of Gr/Re^2. For low R/L, high Gr/Re^2 and high Pr values, the overall heat transfer on the convex surface is greater than the overall heat transfer in a straight channel of equal height. However, when compared on an equal heated area basis, the convex surface has lower heat transfer. For channels with concave walls, where the decrease in cross-sectional area and buoyancy both accelerate the flow, separation is not observed, and considerably greater heat transfer rates are obtained. The overall heat transfer on the concave surface is always greater than a straight channel of equal height. However, when compared to a straight channel of equal heated surface area, there is a critical Gr/Re^2 value below which heat transfer enhancement is obtained with concave surfaces.

1. Introduction

There are a variety of applications involving flow in passages bounded by a curved surface on one side where buoyancy effects are important due to temperature differences between a heated surface and the fluid. Such applications include flow in coolant passages adjoining hot contoured nozzle sections, flow in dome shaped reactors, and flows in chimneys, afterburners, and hot transition sections. They could also be of interest in applications such as energy conservation in buildings aiming to maximize or minimize heat transfer with innovative designs and architecture. However, the majority of the studies dealing with forced, free or mixed convection have been confined to channel and pipe geometries, and there is an extensive body of literature on this topic [1–8]. Mixed convection in channels with curved entry-surfaces has not been seriously investigated, and represents the focus of the present investigation. The geometry selected in this paper is a

* Corresponding author. Tel.: +1-225-388-5809; fax: +1-225-388-5924.
E-mail address: acharya@me.lsu.edu (S. Acharya).

0017-9310/00/$ - see front matter
PII: S0017-9310(99)00269-0

Nomenclature

C_p	specific heat
CE	function representing curvature effect in Eqs. (10) and (12)
$F_1, \ldots, F_5$	functions appearing in the average Nusselt number correlations
g	gravitational acceleration
Gr_L	Grashof number, $Gr_L \beta \rho_0^2 (T_h - T_0) L^3/\mu^2$
h	heat transfer coefficient, $h = -k\{\frac{dT}{dn}\|_{wall}\}/[T_h - T_0]$
H	dimensional height of the hot wall measured from the beginning of the curved surface
k	fluid thermal conductivity
L	inlet width for channel with convex entry, exit width for channel with concave entry
Nu_S	local Nusselt number, $Nu_S = \frac{hS_T}{k}$
$\overline{Nu}$	average Nusselt number, $\overline{Nu} = \frac{1}{S}\int_S Nu_S \, ds$
p	dimensional pressure
P	dimensionless pressure, $P = \frac{P+\rho_0 g y}{\rho_0 v_0^2}$
Pe	Peclet number, $Pe = Re_L Pr$
R	radius of curvature
R/L	aspect ratio
R^*/L	$(\frac{R}{L})^* = 1 + \frac{1}{R/L}$
Re	Reynolds number, $Re = \rho_0 v_0 L/\mu$
Pr	Prandtl number, $Pr = \mu C_p/k$
s, S	dimensional and dimensionless path length along the hot curved wall measured from the beginning of the curved surface
S_T	total length of the hot curved wall
T	dimensional temperature
T_0	dimensional inlet temperature
T_h	dimensional wall temperature of the heated surface
u, v	dimensional velocity components in the cross-stream and streamwise directions
v_0	mean inlet velocity in the streamwise direction
U, V	dimensionless velocity components, $U = u/v_0$, $V = v/v_0$
x, y	dimensional coordinates in the cross-stream and streamwise directions
X, Y	dimensionless coordinates, $X = x/L$, $Y = y/L$

Greek symbols

β	thermal expansion coefficient
ξ, η	boundary-fitted curvilinear coordinates
μ	dynamic viscosity
ρ, ρ_0	density and reference density
θ	dimensionless temperature, $\theta = (T - T_0)/(T_h - T_0)$

generic configuration (not specific to any application) of a curved heated surface bounded by a vertical adiabatic wall. As noted above, heated curved walls are encountered in a number of applications, and a goal of this work is to evaluate and compare the heat transfer on the curved surface with that on an equivalent vertical flat surface. The flow and heat transfer in channels with curved surfaces are expected to be more complex due to changes in flow cross-sectional area and the potential for flow separation.

There is a large body of literature involving separated forced convection past backsteps (see, for example, [9,10]). However, buoyancy has been ignored in these studies. A few related studies involving mixed convection in separated flows have, however, been reported. Acharya and Habchi [11] studied laminar mixed convection heat transfer in a partially blocked, vertical channel. Abu-Mulaweh et al. [12] investigated experimentally laminar mixed convection behind a two-dimensional backward-facing step for the buoyancy-opposing case. Thereafter, Abu-Mulaweh et al. [13] reported measurements of buoyancy-assisting, laminar mixed convection flow of air along a two-dimensional, vertical backward-facing step. The effects of inclination angle and Prandtl number in the same geometry were reported by Hong et al. [14].

Work has also been reported on forced convection past curved surfaces. Concave curvature is known to destabilize laminar boundary layers resulting in Gortler vortices. These vortices appear around a critical Gortler number, and lead to three-dimensional effects that can influence the transition process both favorably and adversely depending on freestream turbulence and geometry. Kestoras and Simon [15] and Finnis and Brown [16] provide a perspective on the various work reported in this area. However, no work on curved surfaces has been reported where buoyancy effects have also been included.

Recently, Moukalled et al. [17] reported numerical results for mixed convection in channels with concave and convex surfaces subjected to favorable and unfa-

vorable pressure gradients. However, this study was reported for a fixed Reynolds number (Re) and Prandtl number (Pr) value. It is the objective of this study to extend the work in [17], and to analyze the effects of Prandtl and Reynolds numbers on the heat transfer characteristics of laminar mixed convection heat transfer in vertical channels with convex and concave entry surfaces. The primary focus of this paper is the influence of streamwise curvature on the surface heat transfer for a range of Reynolds number, Prandtl number and surface curvature. Only two-dimensional laminar flow has been considered in this paper, and the potential development of three-dimensional instabilities leading to early transition to turbulence has been ignored. This assumption is made based on the argument that geometry plays a critical role in dictating the onset and amplification of Gortler vortices and three-dimensional instabilities, and experiments or three-dimensional time- and space-accurate simulations are needed for determining the critical parameters beyond which the three-dimensional effects and transition to turbulence becomes important. In the absence of such experiments or simulations, the simplifying assumption of two-dimensional and laminar flow has been made, and parametric effects have been investigated.

2. Governing equations

The physical situation considered is illustrated schematically in Fig. 1. The curved wall is maintained at a uniform temperature T_h which is higher than that of the inlet flow temperature T_0 ($T_0 < T_h$). The working fluid enters the channel from the bottom with a parabolic-velocity profile representing flow development upstream of the channel entrance.

The governing equations are those expressing the conservation of mass, momentum, and energy. As noted earlier, the flow is considered to be steady, laminar and two-dimensional. Constant thermal properties are assumed except for the density in the body force term of the y-momentum equation which is modeled by the Boussinesq approximation. The non-dimensional forms of the governing conservation equations can be written as

$$\nabla \cdot \vec{V} = 0 \tag{1}$$

$$\begin{aligned} (\vec{V}\cdot\nabla)U &= -\frac{\partial P}{\partial X} + \frac{1}{Re}\nabla^2 U; \\ (\vec{V}\cdot\nabla)V &= -\frac{\partial P}{\partial Y} + \frac{1}{Re}\nabla^2 V + \frac{Gr_L}{Re^2}\theta \end{aligned} \tag{2}$$

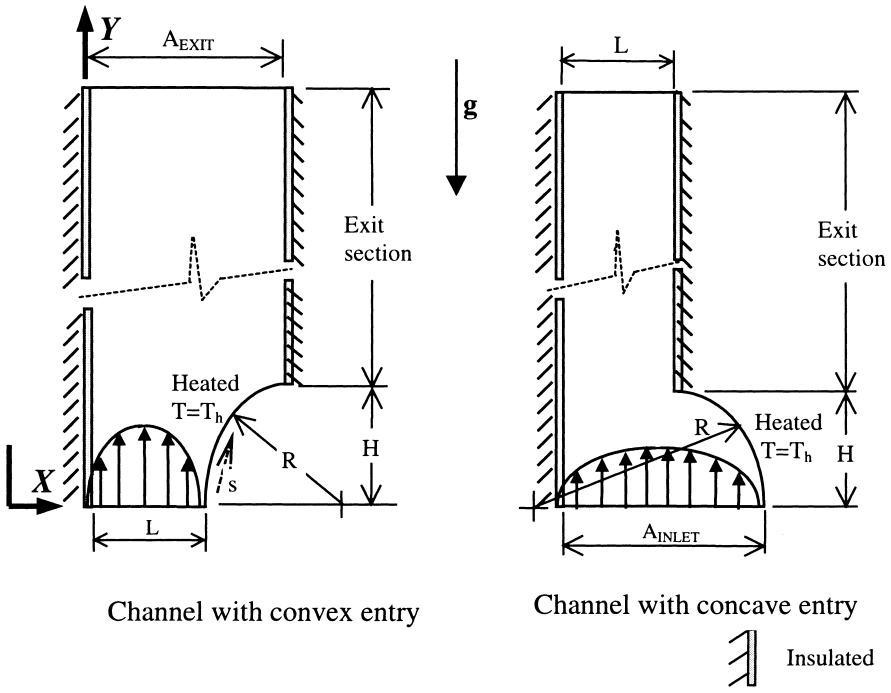

Fig. 1. Schematic of a channel with convex and concave entry.

$$(\vec{V}\cdot\nabla)\theta = \frac{1}{Pe}\nabla^2\theta \tag{3}$$

The boundary conditions used are:

$$V_{in} = 6(X - X^2),\ U_{in} = \theta = 0 \text{ at inlet, and}$$
$$\frac{\partial U}{\partial Y} = \frac{\partial V}{\partial Y} = \frac{\partial \theta}{\partial Y} = 0 \text{ at the exit} \tag{4}$$

$$U = V = 0,\ \theta = 1 \text{ along the heated wall, and}$$
$$U = V = \frac{\partial \theta}{\partial X} = 0 \text{ along the insulated walls} \tag{5}$$

The boundary conditions at the inlet and exit correspond to the case where the heated curved section is located between an inlet duct and an exit duct. Thus, flow entering the curved section is assumed to be fully developed (permitting the use of a parabolic velocity profile at the inlet). The flow exiting the downstream development duct is also considered to be fully developed (permitting the use of zero-gradient condition). The exit section of the channel is made long enough so that ther is no reverse flow at the channel exit, and the outflow zero-gradient boundary condition can be safely applied.

3. Solution procedure and computational detail

The control volume approach is adopted to solve the coupled system of equations governing the flow and temperature fields (Eqs. (1)–(3)) numerically. The discretized form of the equations are obtained by first expressing Eqs. (1)–(3) using a general curvilinear coordinate system (ζ, η), and then integrating the resulting equations over each control volume. The integrated equations are reduced to algebraic equations by expressing the variation in the dependent variable and its derivatives in terms of the grid point values using the power law scheme of Patankar [18]. The resulting system of algebraic equations is solved by a line-by-line Thomas algorithm [18]. The unknown pressure field is obtained using the SIMPLE algorithm of Patankar and Spalding [19]. Solutions are obtained over a non-staggered grid in which the checkerboard pressure and velocity fields are eliminated through the use of the Pressure Weighted Interpolation Method (PWIM) of Peric [20]. All computations are performed using non-uniform grids with denser clustering near the walls where boundary layers develop and high gradients are expected. The grid is generated using the transfinite interpolation technique [21].

To investigate the sensitivity of the solution to the grid spacing used, numerical studies were carried out in the channels with convex and concave entry on several non-uniform grids and the computed average Nusselt number values are shown in Table 1. As a compromise between accuracy and CPU time, the 31×81 and 51×231 grid systems are respectively used for all calculations in channels with concave and convex entry. The much larger number of streamwise points in the channel with convex entry was due to a longer exit section for the channel associ-

Table 1
Grid size tests

Concave entry channel				
Grid size	21×51	31×81	51×101	Maximum difference
	Average Nusselt numbers			
$Gr/Re^2 = 0.1$	9.46	9.31	9.35	0.43%
$Gr/Re^2 = 1.0$	9.77	9.69	9.71	0.21%
$Gr/Re^2 = 3.0$	10.53	10.42	10.44	0.19%
$Gr/Re^2 = 5.0$	11.08	11.02	10.99	0.29%
Convex entry channel				
Grid size	31×231	51×231	51×281	Maximum difference
	Average Nusselt numbers			
$Gr/Re^2 = 0$	7.68	7.66	7.64	0.52%
$Gr/Re^2 = 0.1$	7.71	7.7	7.68	0.39%
$Gr/Re^2 = 1.0$	8.69	8.73	8.76	−0.8%
$Gr/Re^2 = 3.0$	10.25	10.24	10.3	0.49%
$Gr/Re^2 = 5.0$	11.2	11.13	11.2	0.63%

ated with flow separation and the numerical requirement of specifying an outflow boundary condition.

As a further check for accuracy, the velocity and temperature profiles across a vertically oriented, asymmetrically heated straight channel computed by Habchi and Acharya [8] and Aung and Worku [3] are compared against profiles obtained by the present code using the same flow parameters (Fig. 2). The various sets of results compare very well and are nearly identical, confirming the credibility of the grid size used and the solution procedure and algorithm employed.

4. Results and discussion

The parameters affecting heat transfer in this study are the Reynolds number Re, the Prandtl number Pr, the curvature ratio R/L, and the Grashof number Gr. Seven values of $Re\,(100 \leq Re \leq 1000)$ and 10 values of $Pr\,(0.72 \leq Pr \leq 50)$ are considered for each value of Gr/Re^2 and R/L. The values of R/L are varied from 1.04 to ∞ while those of Gr/Re^2 are varied between 0 and 5. In order to reveal the effects of the various parameters on heat transfer, results are presented in terms of streamline and isotherm plots, velocity and tempera-

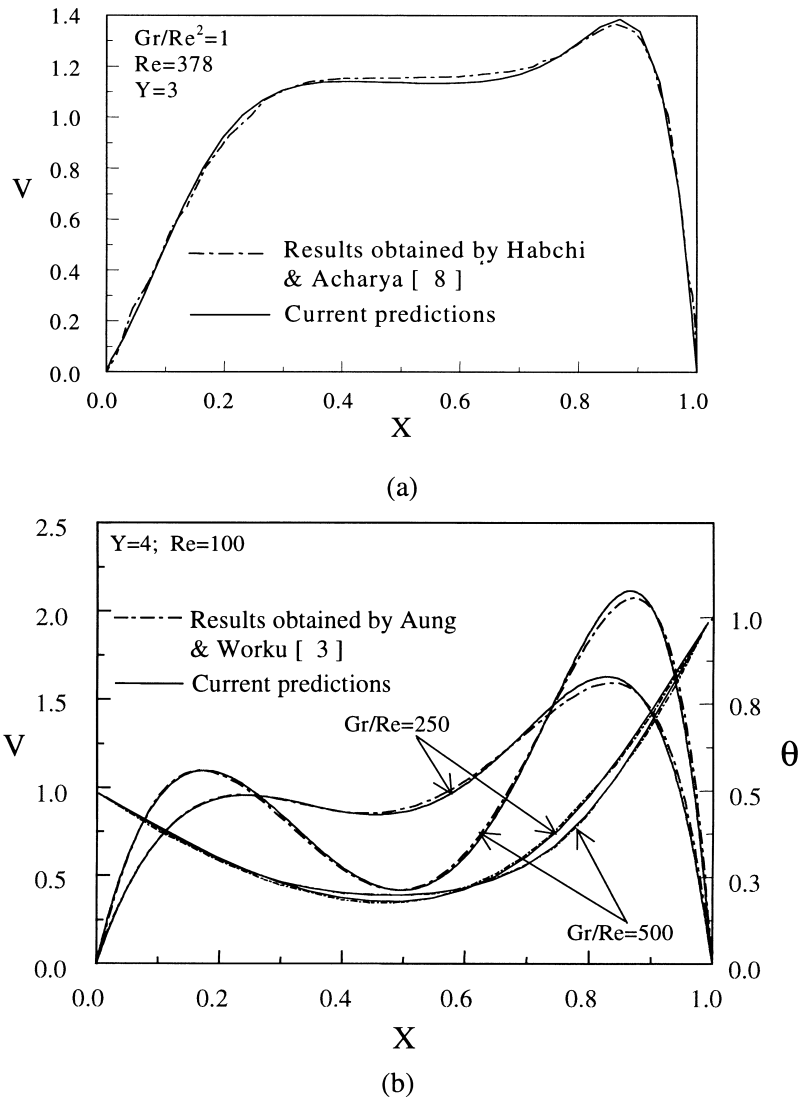

Fig. 2. (a) Velocity distribution across a straight channel heated from one side; (b) velocity and temperature distribution across a straight channel heated asymmetrically from both sides ($\theta = 0.5$ (left), $\theta = 1$ (right)).

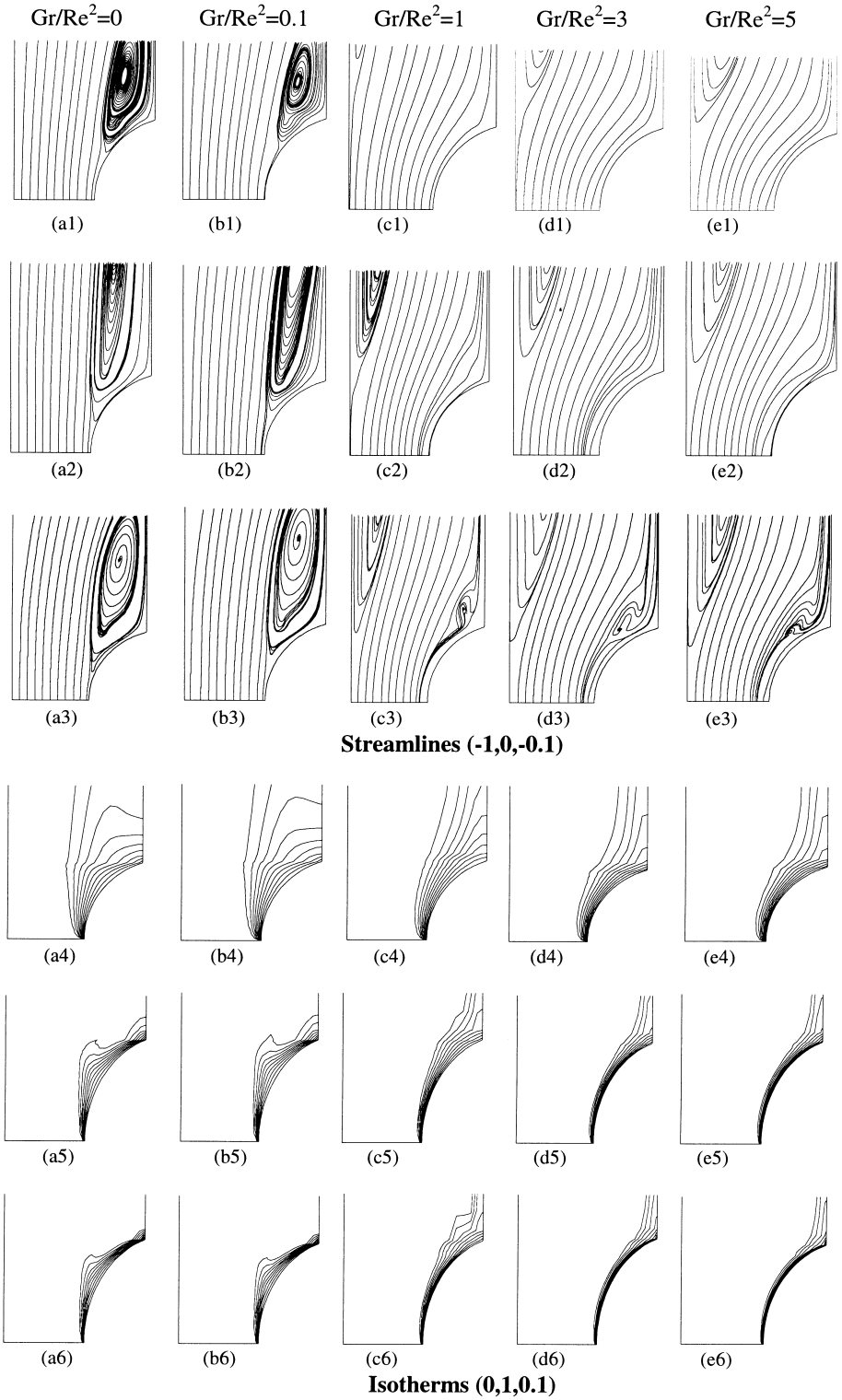

Fig. 3. Streamline and isotherm plots for convex entry at $Pr = 0.72$ and $R/L = 1.04$, at $Re = 100$ ((a1)–(e1) and (a4)–(e4)), $Re = 500$ ((a2)–(e2) and (a5)–(e5)), and $Re = 1000$ ((a3)–(e3) and (a6)–(e6)).

ture profiles, and local and average Nusselt number values.

5. Channels with convex entry

5.1. Effects of Reynolds number

5.1.1. Streamlines and isotherms

Fig. 3 shows streamline plots for different values of Gr/Re^2 at $Re = 100$, 500, and 1000 ($R/L = 1.04$). At low Gr/Re^2, buoyancy effects are weak, and separation occurs at the exit from the heated convex section due to the expansion in the cross-sectional area of the channel. As Gr/Re^2 increases, buoyancy effects accelerate the fluid near the heated wall causing the separation near the heated wall to disappear. This elimination of the separation region occurs between Gr/Re^2 of 0.1 and 1 for the Re range between 100 and 1000. Since the mass flow rate in the channel is constant, acceleration of the flow near the heated surface leads to a deceleration and eventual flow separation adjacent to the insulated vertical wall.

The influence of Reynolds number can be assessed by comparing the plots of a particular column in Fig. 3 (Pr is fixed at 0.72). In view of the higher velocity at $Re = 500$, the recirculation zone along the heated surface, shown in Fig. 3(a2)–(e2), are larger and stronger as compared with those in Fig. 3(a1)–(e1). As Re is raised to 1000 (Fig. 3(a3)–(e3)), a further increase in the size of the recirculation cells is noted. The stronger separation at the higher Re is due to the higher adverse pressure gradients associated with the area expansion in the channel. At higher Re values, the reduction or elimination of the flow separation adjacent to the heated surface is delayed to higher Gr/Re^2 (since a stronger buoyancy force is required to overcome the greater adverse pressure gradients), and at the same time, the separation adjacent to the insulated vertical surface becomes larger. This can be seen clearly at $Re = 1000$, where the signature of the separation near the hot wall remains even at $Gr/Re^2 = 5$. This implies that even at this large value of Gr/Re^2, the buoyancy forces are not strong enough to completely overcome the adverse pressure gradients at $Re = 1000$. However, as at lower Re, the change in flow structure from flow separation near the curved heated wall to separation on the opposite vertical wall occurs primarily between Gr/Re^2 of 0.1 and 1. For $Gr/Re^2 \geq 1$, the remnants of the separation near the heated surface appears to be in the form of a small vortex near the exit of the curved section and lifted slightly away from the heated wall.

The corresponding isotherm plots for the above cases are presented in Fig. 3(a4)–(e6). As shown, the thermal boundary layer decreases in thickness as the Reynolds number increases. This is revealed by the denser concentration of isotherms near the hot wall. In regions where flow separation begins, the isotherms diverge reflecting a decrease in heat transfer associated with the onset of separation. This can be seen in all the isotherm plots where a separation along the heated surface exists, and is expectedly more evident when the separation is stronger. However, despite this initial decrease in heat transfer following the onset of separation, the temperature gradients and heat transfer again increases further downstream in the separation region. This is due to the separated eddy which impinges back on the curved surface beyond the location of separation. The divergence of the isotherms with the onset of separation followed by a convergence of the isotherms further downstream leads to somewhat distorted isotherm contours that are evident in Fig. 3(a5), (b5), (a6), and (b6).

5.1.2. Velocity and temperature distributions

The streamwise velocity distributions (non-dimensionalized with the mean inlet velocity) for selected cases are shown in Fig. 4(a)–(c). Fig. 4(a) shows the velocity profiles across the mid-height of the curved portion of the channel for different values of Re ($Pr = 0.72$ and $Gr/Re^2 = 0.1$). This location is just upstream of the onset of flow separation. As shown, increasing Re has almost no effect on the general shape of the velocity distribution at low values of Gr/Re^2, and forced convection effects essentially dominate. The only observable difference is that the velocity near the heated surface is lower at the higher Re and is due to the associated higher pressure gradients. On the other hand, Fig. 4(b) (at $Y = 0.5$) and Fig. 4(c) (at $Y = 0.9$) show that for high values of Gr/Re^2 ($=5$), buoyancy induced acceleration near the heated surface produces a local velocity peak near the heated wall. For the highest Re ($=1000$), the near-wall boundary layer is the thinnest, and the buoyancy induced peak is closest to the heated surface. The differences in the near-wall velocity profiles for the different Re values (at the same value of Gr/Re^2) also indicate the importance of Re as an independent parameter. At lower values of Re, the same value of Gr/Re^2 appears to provide a stronger flow acceleration near the heated wall. In Fig. 4(b) and (c), there is a local minimum in the velocity profile just beyond the location of the near-wall peak, and is presumably associated with the combined effects of flow rate reduction away from the wall to compensate for flow acceleration near the wall, and the signature of the flow recirculation near the heated wall (evident in the contour plot in Fig. 3(e3)). At a higher Re, these effects are stronger, and the local

minimum is more accentuated as seen in Fig. 4(b) and (c). In Fig. 4(c), evidence of flow separation on the adiabatic wall ($X = 0$) can be observed at the highest Re.

The influence of Re on the temperature distribution for $Gr/Re^2 = 0.1$ and 5 can be seen in Fig. 4(d) and (e), respectively. These curves reflect the isotherm plots presented in Fig. 3. As stated earlier, the thermal boundary layer thickness decreases as Re increases. Therefore, as Re is increased, steeper temperature gradients are obtained resulting in higher heat transfer rates. Fig. 4(d) depicts the effect of Re on the temperature distribution near the exit of the channel ($Y = 0.9$) at a value of $Gr/Re^2 = 0.1$. The flow separation introduces thermal distortion close to the hot wall, and as shown in Fig. 3, this effect is stronger at a higher Re value. However, as the strength of buoyancy forces or Gr/Re^2 increases, the recirculation bubble near the heated wall diminishes (Fig. 3), and for $Gr/Re^2 = 5$, a profile as shown in Fig. 4(e) is obtained, with no thermal distortion in the profiles.

5.1.3. Nusselt numbers

The heat transfer effectiveness of the channel is displayed in terms of local and average Nusselt number values. The effects of varying Re on local Nusselt number (Nu_S) along the hot wall are illustrated for $Gr/Re^2 = 0.1$ and 5 in Fig. 4(f) for a Pr value of 0.72. As the flow develops and the bulk fluid gets heated, the Nusselt number profiles expectedly decrease from their high values near the channel inlet. In general, the level of Nu_S increases with Re due to the thinning of the near-wall boundary layer and increase of the wall temperature gradients. At Gr/Re^2 of 5, as seen in Fig. 3, no separation is observed near the heated wall for $Re = 100$ and 500, and for these cases the Nu_S profile is monotonic. For $Re = 1000$, the signature of flow separation persists near the exit of the curved section, and this manifests itself in the Nu_S profile as a sudden dip (near S of 1) followed by an increase. At $Gr/Re^2 = 0.1$, the separation near the heated curved surface is present for all Re, and becomes stronger with increasing Re. Recall that in the isotherm plots,

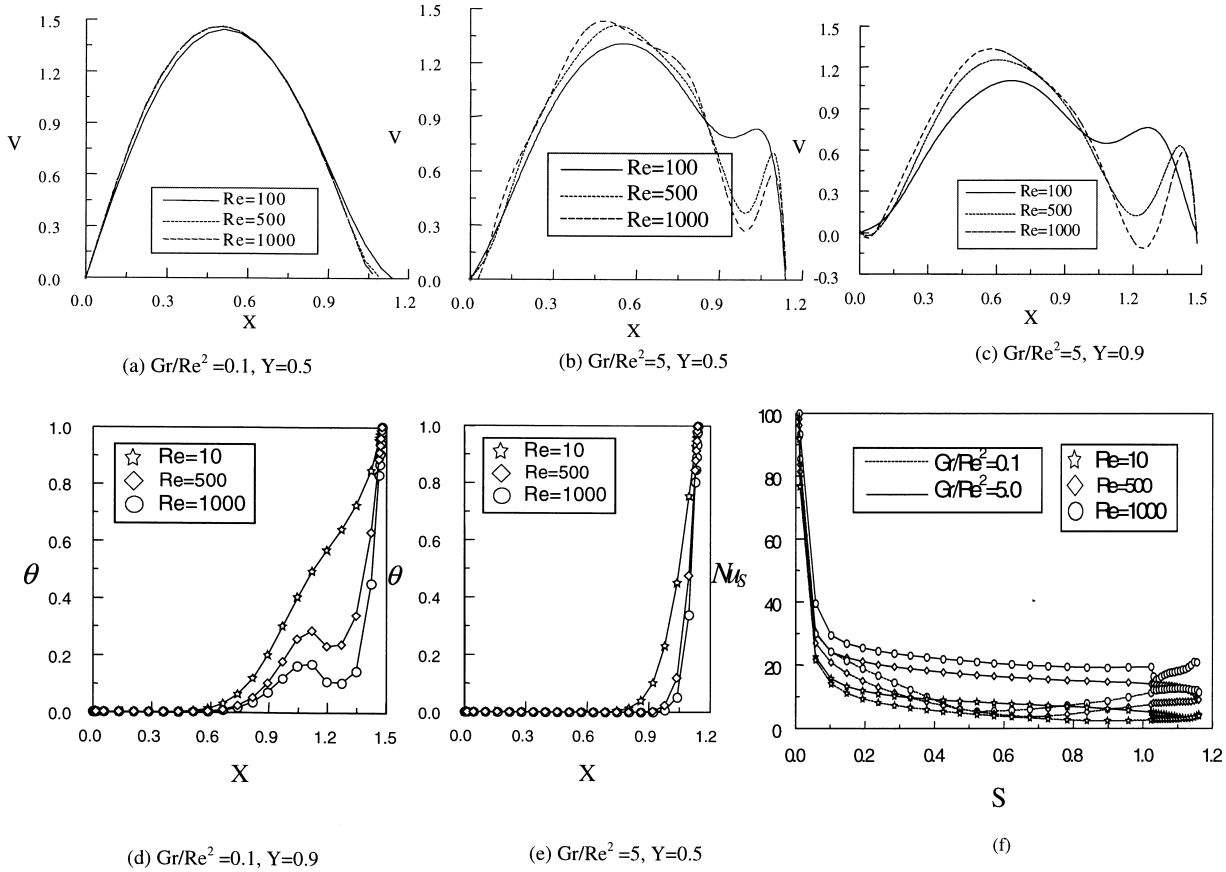

(a) Gr/Re^2 =0.1, Y=0.5 (b) Gr/Re^2=5, Y=0.5 (c) Gr/Re^2=5, Y=0.9

(d) Gr/Re^2 =0.1, Y=0.9 (e) Gr/Re^2 =5, Y=0.5 (f)

Fig. 4. (a)–(c) Velocity, (d), (e) temperature, and (f) Nusselt number distribution for different values of Re (convex entry; $R/L = 1.25$, $Pr = 0.72$).

Table 2
Average Nusselt number of the heated wall for all considered values of Re ($Pr = 0.72$)

Gr/Re^2	Re						
	100	200	300	400	500	800	1000
			$R/L = 1.04$, $H = 1$, $S = 1.34$ (channel with convex entry)				
0	7.68	8.95	10.09	11.04	11.87	14.0	15.38
0.1	7.71	8.91	9.97	10.86	11.61	13.63	15.15
1	8.69	10.25	11.5	12.62	13.65	16.44	18.11
3	10.25	12.83	14.98	16.91	18.69	22.95	25.03
5	11.2	14.37	17.01	19.34	21.35	25.89	28.09
			$R/L = 1.04$, $H = 1$, $S = 1.34$ (channel with concave entry)				
0	9.52	11.92	13.93	15.64	17.15	20.83	22.82
0.1	9.57	12.02	14.08	15.84	17.51	21.21	23.27
1	9.98	12.88	15.32	17.42	19.28	23.71	26.02
3	10.79	14.39	17.31	19.75	21.84	26.58	28.94
5	11.47	15.52	18.71	21.3	23.47	28.27	30.61
			$R/L = \infty$, $H = 1$, $S = 1$				
0	8.33	9.72	10.74	11.57	12.31	13.98	14.89
0.1	8.39	9.84	10.92	11.81	12.58	14.43	15.42
1	8.83	10.71	12.18	13.39	14.43	16.85	18.06
3	9.60	12.02	13.86	15.33	16.53	19.2	20.51
5	10.18	12.93	14.93	16.49	17.74	20.5	21.86
			$R/L = \infty$, $H = 1.34$, $S = 1.34$				
0	9.43	11.39	12.67	13.71	14.32	16.71	17.51
0.1	9.46	11.56	12.93	14.06	14.68	17.39	18.24
1	10.11	12.81	14.72	16.31	17.29	20.92	22.08
3	11.16	14.61	17.04	19.0	20.17	24.26	25.46
5	11.93	15.82	18.5	20.61	21.82	26.06	27.27

the onset of separation led to a divergence of isotherms (lower temperature gradients and heat transfer) but further downstream in the separation region, the isotherms converged again leading to higher near-wall gradients and therefore higher heat transfer. These observations are apparent in the Nu_S profiles at $Gr/Re^2 = 0.1$, where a minimum in Nu_S is obtained in the vicinity of a non-dimensional streamwise distance of 0.6 followed by a gradual increase.

Average Nusselt number values over the hot surface are calculated and compared with corresponding estimates obtained in straight channels (Table 2). The comparison is shown only for the highest curvature (lowest aspect ratio, $R/L = 1.04$) case. For this case, the dimensionless path length of the curved surface is 1.34, while the dimensionless height is 1. The first comparison is made with a straight channel of the same height as the curved channel. For this case, the straight channel has a smaller heated area ($S = H = 1$) than the curved channel. The second comparison is with straight channels of heated areas equal to those of the curved channels. In this case, the straight channels have greater height ($H = S = 1.34$) than the curved channels.

Generally, $\overline{Nu}$ increases with increasing Gr/Re^2 and/or increasing Re. This is expected since increasing Gr/Re^2 accelerates the near hot wall fluid and increasing Re increases the inlet velocity and leads to thinner boundary layers. At low Gr/Re^2, values of $\overline{Nu}$ computed in channels with convex entry reveal a reduction in heat transfer rate as compared to the corresponding values computed in straight channels of equal height. This reduction in heat transfer, for $R/L = 1.04$, is due to the separation region near the heated curved surface, and is greater with increasing Re due to the associated increase in the size and strength of the separation along the heated wall. At high values of Gr/Re^2, however (typically between 1 and 3), the separation along the heated curved surface is no longer present and the heat transfer rate of channels with convex entry is higher than that of a straight channel of equal height. This is a direct consequence of the greater surface area for heat transfer and therefore higher buoyancy forces acting over a longer distance. For $R/L = 2.5$ (values not shown in the table), no flow separation is obtained along the heated wall, but the flow decelerates due to an increase in cross-sectional area and leads to a reduction in heat transfer at low values of Gr/Re^2. For this R/L also, the heat transfer degradation on the convex surface changes to heat transfer enhancement for a Gr/Re^2 value between 1 and 3.

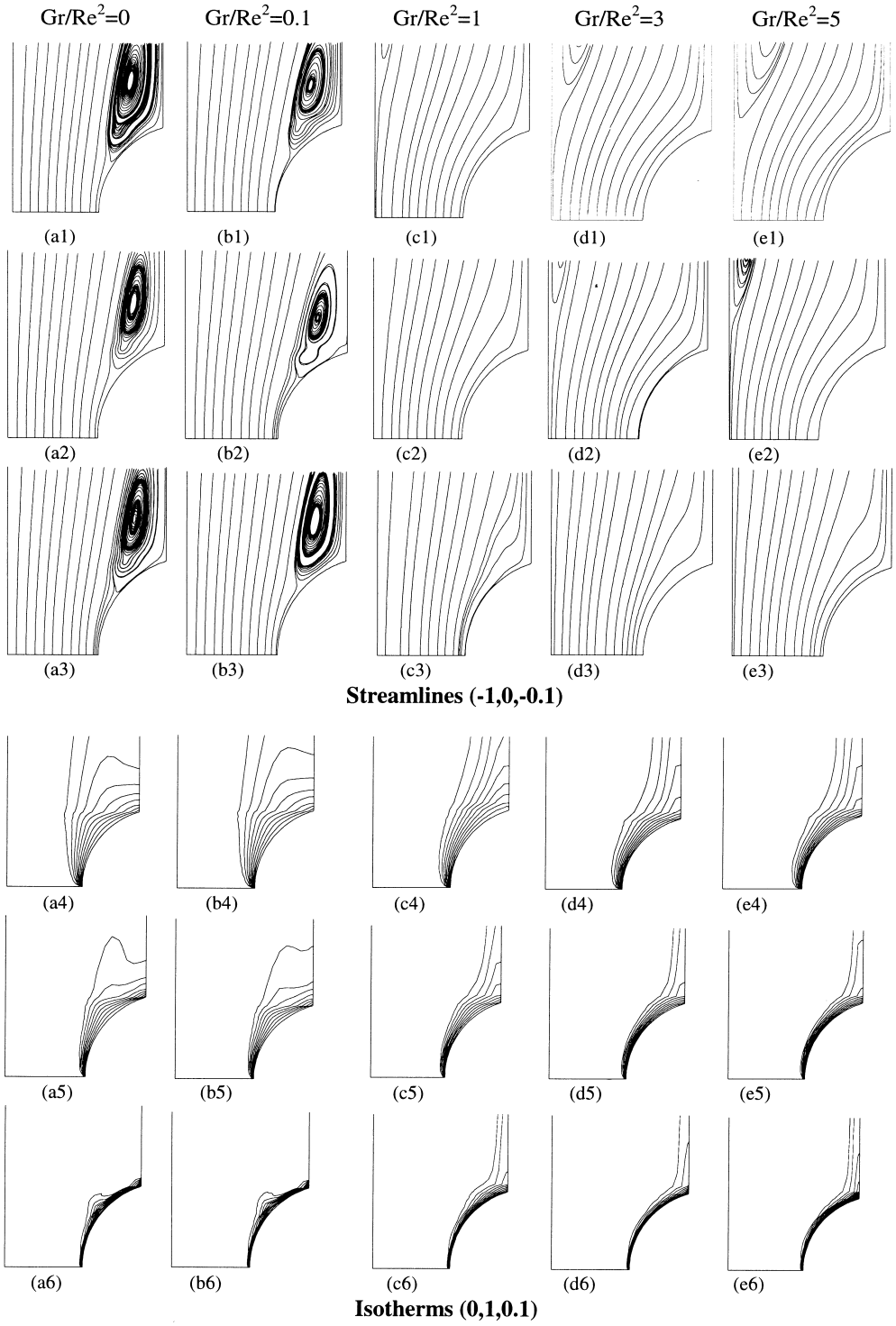

Fig. 5. Streamline and isotherm plots for convex entry at $Re = 100$ and $R/L = 1.04$, at $Pr = 0.72$ ((a1)–(e1) and (a4)–(e4)), $Pr = 3$ ((a2)–(e2) and (a5)–(e5)), and $Pr = 50$ ((a3)–(e3) and (a6)–(e6)).

In comparing with straight channels of heated length equal to the curved channel with convex entry, expectedly for all values of Gr/Re^2, the Nusselt number values obtained for the straight channel are higher than those computed in the curved channel. This is because, in the straight channel, there is no flow separation or deceleration induced by increases in cross-sectional area that occur in the channel with convex entry.

5.2. Effects of Prandtl number

5.2.1. Streamlines and isotherms

Representative streamline plots are displayed in Fig. 5(a1)–(e3) for different values of Pr and Gr/Re^2 at $Re = 100$ and $R/L = 1.04$. At low values of Gr/Re^2, the recirculation region at exit from the curved section is dominated by the adverse pressure gradient effects, and the thinning of the thermal boundary layer with increasing Pr does not appear to greatly influence the separation region. As noted earlier, at $Pr = 0.72$, with increasing values of Gr/Re^2, the flow near the heated surface is accelerated leading to the reduction and elimination of the separation along the heated surface, and resulting in the appearance of a recirculation bubble along the insulated wall. However, as Pr is increased, the corresponding decrease in the fluid conductivity limits the acceleration of the near hot-wall fluid to a thinner thermal boundary layer region. Therefore, the corresponding decrease in velocity away from the hot wall is also reduced, and at $Pr = 50$ separation does not occur on the opposite vertical wall. The corresponding isotherm plots are presented in Fig. 5(a4)–(e6). As expected, the thermal boundary layer decreases in thickness as Pr increases. This is reflected by the denser clustering of isotherms close to the hot curved wall as Pr increases. The spread of isotherms at low values of Pr is due to a strong streamwise conduction that decreases the streamwise temperature gradient in the fluid. The separation-induced distortion of

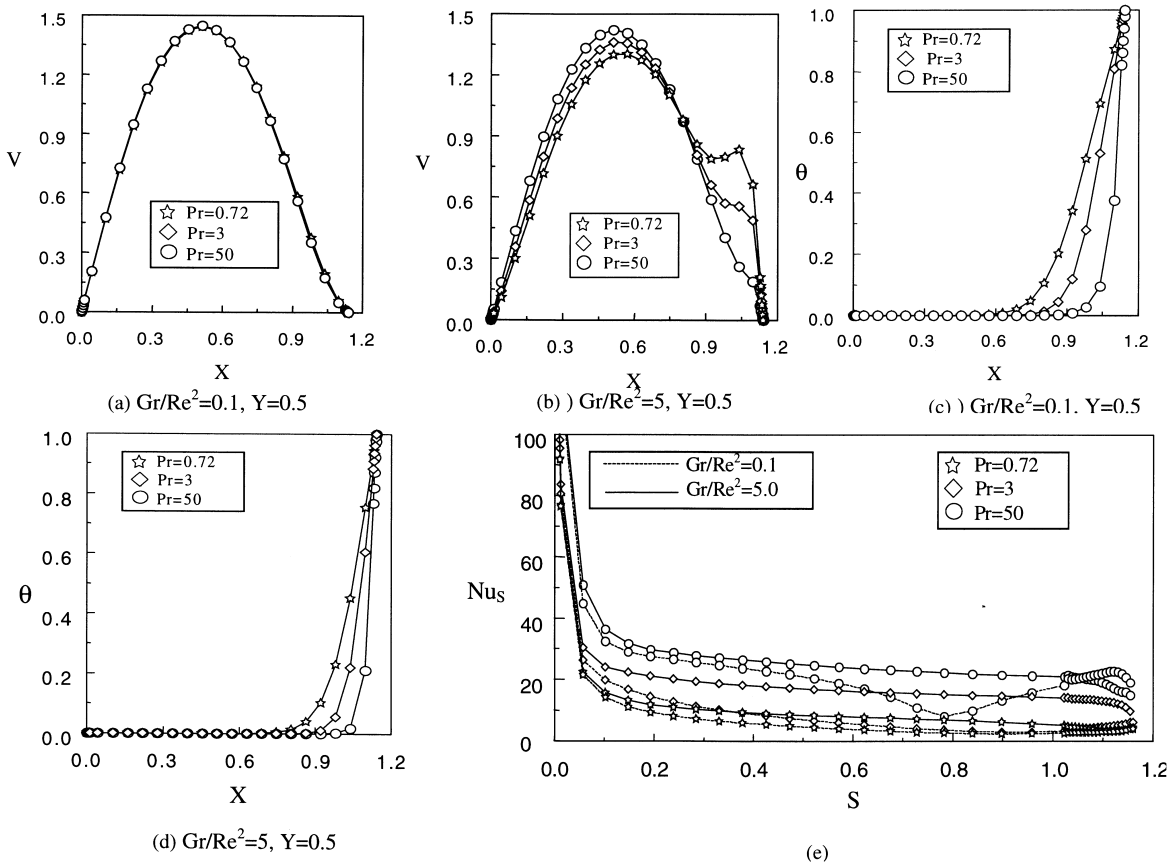

Fig. 6. (a)–(b) Velocity, (c)–(d) temperature, and (e) Nusselt number distribution for different values of Pr (concave entry; $R/L = 1.25$, $Re = 100$).

the isotherms is evident at all Pr, and is more noticeable as Pr increases.

5.2.2. Velocity and temperature distributions

The effects of Prandtl numbers on the velocity profiles across the channel's mid-height are shown in Fig. 6(a) and (b) for $Gr/Re^2 = 0.1$ and 5, respectively. As depicted in Fig. 6(a), increasing Pr has almost no effect on the general shape of the velocity distribution at low values of Gr/Re^2. On the other hand, the Prandtl number value is seen to greatly affect the velocity profiles at higher values of Gr/Re^2 (Fig. 6(b)). Note that Pr appears only in the energy equation. In the pure forced convection situation ($Gr/Re^2 = 0$), the velocity field is unaffected by Pr since there is no coupling between the velocity and temperature field. At low values of Gr/Re^2, the buoyancy source term that couples the velocity and temperature is small and the effects of Pr are correspondingly weak. At high values of Gr/Re^2, the buoyancy source term in the Y-momentum equation is large and variations in its magnitude due to a variation in Pr strongly influence the velocity distribution. Higher Pr implies lower thermal diffusion of heat from the heated surface and lower magnitudes of the buoyancy source term and buoyancy induced flow acceleration. This explains the differences in profiles obtained at high values of Gr/Re^2 for different values of Pr.

Fig. 6(c) and (d) illustrate the influence of Pr on temperature distribution across the mid-height of the channel for low and high values of Gr/Re^2, respectively. Unlike velocity, temperature profiles are affected by Pr even at low values of Gr/Re^2. This is to be expected since Pr is an important parameter in the energy equation and its effects are always present independent of the magnitude of buoyancy forces. The various curves in Fig. 6(c) and (d) show that temperature gradients are higher at higher Pr values due to a decrease in the thermal boundary layer thickness. Furthermore, it can be inferred from the figures that the effects of Pr on the temperature profiles decrease with increasing values of Gr/Re^2. Higher Gr/Re^2 values imply higher velocities and higher advective heat transfer coefficients. Thus, the effects of Pr or thermal diffusion diminish in the wake of increasing advection effects.

Table 3
Average Nusselt number of the heated wall for all considered values of Pr ($Re = 100$)

Gr/Re^2	Pr									
	0.72	2	3	5	7.5	10	15	25	35	50
				$R/L = 1.04$, $H = 1$, $S = 1.34$ (channel with convex entry)						
0	7.68	9.57	10.7	12.46	14.13	15.46	17.54	20.48	22.6	24.98
0.1	7.71	9.51	10.6	12.31	13.96	15.28	17.32	20.23	22.32	24.68
1	8.69	10.73	11.79	13.37	14.82	15.98	17.75	20.27	22.05	25.19
3	10.25	13.01	14.39	16.41	18.25	19.68	21.87	24.84	26.88	29.06
5	11.2	14.41	16.0	18.28	20.34	21.92	24.25	27.25	29.33	31.34
				$R/L = 1.04$, $H = 1$, $S = 1.34$ (channel with concave entry)						
0	9.52	12.59	14.27	16.85	19.26	21.17	24.15	28.43	31.56	35.02
0.1	9.57	12.68	14.38	16.98	19.41	21.33	24.32	28.6	31.71	35.15
1	9.98	13.42	15.28	18.07	20.64	22.64	25.71	29.95	32.93	36.14
3	10.79	14.79	16.88	19.94	22.67	24.76	27.87	31.99	34.75	37.68
5	11.47	15.88	18.12	21.33	24.15	26.26	29.34	33.33	35.96	38.72
				$R/L = \infty$, $H = 1$, $S = 1$						
0	8.33	10.53	11.73	13.46	15.08	16.36	18.31	20.94	22.65	24.45
0.1	8.39	10.62	11.83	13.57	15.2	16.48	18.43	21.03	22.73	24.51
1	8.83	11.31	12.61	14.45	16.14	17.43	19.34	21.8	23.4	25.07
3	9.60	12.43	13.88	15.85	17.58	18.85	20.69	22.96	24.44	26.02
5	10.18	13.27	14.80	16.84	18.58	19.84	21.61	23.8	25.21	26.75
				$R/L = \infty$, $H = 1.34$, $S = 1.34$						
0	9.43	12.27	13.61	15.76	17.87	19.46	21.95	25.42	27.81	30.09
0.1	9.46	12.4	13.7	15.92	18.05	19.65	22.14	25.6	27.96	30.31
1	10.11	13.4	14.8	17.15	19.4	21.04	23.53	26.85	29.06	31.15
3	11.16	14.89	16.52	19.08	21.46	23.13	25.58	28.69	30.71	32.63
5	11.93	16.0	17.76	20.43	22.88	24.55	26.94	29.92	31.85	33.69

5.2.3. Nusselt numbers

Representative plots showing the effects of Pr on local Nusselt number (Nu_S) distribution along the hot wall are displayed in Fig. 6(e) for a channel of aspect ratio $R/L = 1.25$ and for two different values of Gr/Re^2 of 0.1 and 5. In general, the level of Nu_S increases significantly as Pr increases. This behavior is due to higher temperature gradients along the wall associated with higher values of Pr. For a Gr/Re^2 of 0.1, Fig. 4 ($Pr = 0.72$) had indicated an increase in Nusselt number toward the exit of the convex section following a minimum at an S value of about 0.6. This behavior was linked to the re-convergence of isotherms toward the trailing edge of the separation. A similar behavior is observed in Fig. 6(e) for all three Pr, except that the behavior is considerably more accentuated at $Pr = 50$.

The overall heat transfer results ($\overline{Nu}$) for different values of Pr in channels with convex entry (and for $R/L = 1.04$) are compared with corresponding values obtained in a straight channel of equal height and straight channels of equal heated lengths in Table 3. $\overline{Nu}$ increases significantly with increasing Pr, and is due to a decrease in the thermal boundary layer thickness with a consequent increase in the temperature gradient as Pr increases. Comparing the curved channel heat transfer rates with those of a straight vertical channel of equal height, it is apparent that the curved channel heat transfer rates are higher only for high Gr/Re^2 and Pr values. For $R/L = 1.04$, the curved channel heat transfer rates are higher only for $Pr = 50$ for $Gr/Re^2 \leq 1$ and for all Pr for $Gr/Re^2 \geq 3$. At $R/L = 1.25$, the parameter window for which enhancement occurs is reduced, and for $R/L = 2.5$ no enhancement is noted. When comparing with straight channels of equal heated surface area, the curved channel with convex entry always has lower heat transfer rates.

5.3. Average Nusselt number correlations

The average Nusselt number over the heated surface has been correlated as the product of two functions, one, that is a function of the flow parameters Re, Gr/Re^2, Pr, and the other that is a function of the curvature or the aspect ratio R/L. Note that once R/L is specified, the height of the curved surface H and the heated length S can be both uniquely determined, and therefore, do not have to be directly incorporated in the correlations. Thus, the average Nusselt number is expressed as:

$$\overline{Nu} = \overline{Nu}_{SC} \times CE \tag{6}$$

where CE is the curvature effect and $\overline{Nu}_{SC}$ is a correlation that has the same functional form as a straight channel correlation [22], and contains the flow parameters Pr, Re, and Gr/Re^2. The correlation for $\overline{Nu}_{SC}$ is expressed as:

$$\overline{Nu}_{SC} = 6.85F_1(Pr)Re^{1/4}F_2\left(Pr, \frac{Gr}{Re^2}\right)Pr^{-0.1} \tag{7}$$

where

$$F_1(Pr) = 0.399\ Pr^{1/3}\left[1 + \left(\frac{0.0468}{Pr}\right)^{2/3}\right]^{-1/4};$$
$$F_2\left(Pr, \frac{Gr}{Re^2}\right) = \left\{1 + \left[\frac{2}{3}\frac{F_3(Pr)}{F_1(Pr)}\left(\frac{Gr}{Re^2}\right)^{1/4}\right]^2\right\}^{1/2} \tag{8}$$

and

$$F_3(Pr) = \frac{3}{4}Pr^{1/2}\left[2.5\left(1 + 2Pr^{1/2} + 2Pr\right)\right]^{-1/4} \tag{9}$$

The correlation for the curvature effect CE is given by the following expression

$$CE = 0.0075 \times F_4\left[\left(\frac{R^*}{L}\right)\right] \times EGR^{0.13} \times Pr^{0.01} \tag{10}$$

where

$$EGR = 1 + \frac{\left(Gr/Re^2\right)^{3/2} + Re^{0.3}}{(R/L)};$$
$$F_4\left[\left(\frac{R}{L}\right)^*\right] = \left\{172 - 104\left(\frac{R}{L}\right)^* + 32\left[\left(\frac{R}{L}\right)^*\right]^2\right\}^2;$$
$$\left(\frac{R}{L}\right)^* = 1 + \frac{1}{R/L}$$

The above correlation is valid to within 15%.

6. Channels with concave entry

The channel with concave entry represents a situation where the cross-sectional area changes aid buoyancy effects. Streamline and isotherm contours are not presented for this case, but it should be noted that no flow separation is noted in this situation, since the cross-sectional area of the channel decreases in the streamwise direction. The effect of the various parameters is presented through a comparison of the velocity, temperature and Nusselt number line plots, and tables of average Nusselt number values.

6.1. Effects of Reynolds number

6.1.1. Velocity and temperature distributions

Fig. 7(a) shows the velocity profiles across the mid-

height of a concave surface of curvature ratio $R/L = 1.25$ for different values of Re ($Gr/Re^2 = 5$ and $Pr = 0.72$). The behavior shown in Fig. 7(a) is similar to that of Fig. 4(b), but with more modest parametric effects. Recall that for convex entry, these effects had been attributed to the combined effects of flow separation, and near wall flow acceleration with associated reduction in flow away from the wall. In the present case, with concave channel entry, there is no flow separation, and so, only the flow acceleration effects are prominent. However, in the present case, the flow acceleration is not limited to the heated surface (where buoyancy-induced acceleration takes place) but flow accelerates across the entire cross-section due to a decrease in the cross-sectional area downstream. Therefore, at the exit from the curved concave section (Fig. 7(b)), the effects of flow reduction away from the wall are minimized.

Fig. 7(c) illustrates the influence of Re on the temperature distribution across the mid-height of the same channel at $Gr/Re^2 = 5$ and $Pr = 0.72$. The thermal boundary layer thickness decreases as Re value increases, leading to higher near wall temperature gradients. The near-wall gradients are greater relative to the convex entry case since the near-wall flow acceleration is stronger for the concave entry case with the flow aided by both decreasing cross-section and buoyancy.

6.1.2. Nusselt numbers

The effects of varying Re on local Nusselt number (Nu_S) variation along the hot wall are illustrated in Fig. 7(d). Re appears to have significant effect on Nu_S in the channel with concave entry at both low and high values of Gr/Re^2. For a given Gr/Re^2, the level of Nu_S increases with increasing Re due to the associated higher near wall velocity and temperature gradients (Fig. 7(a)–(c)). Moreover, as the flow approaches the exit, the decrease in the channel's cross-sectional

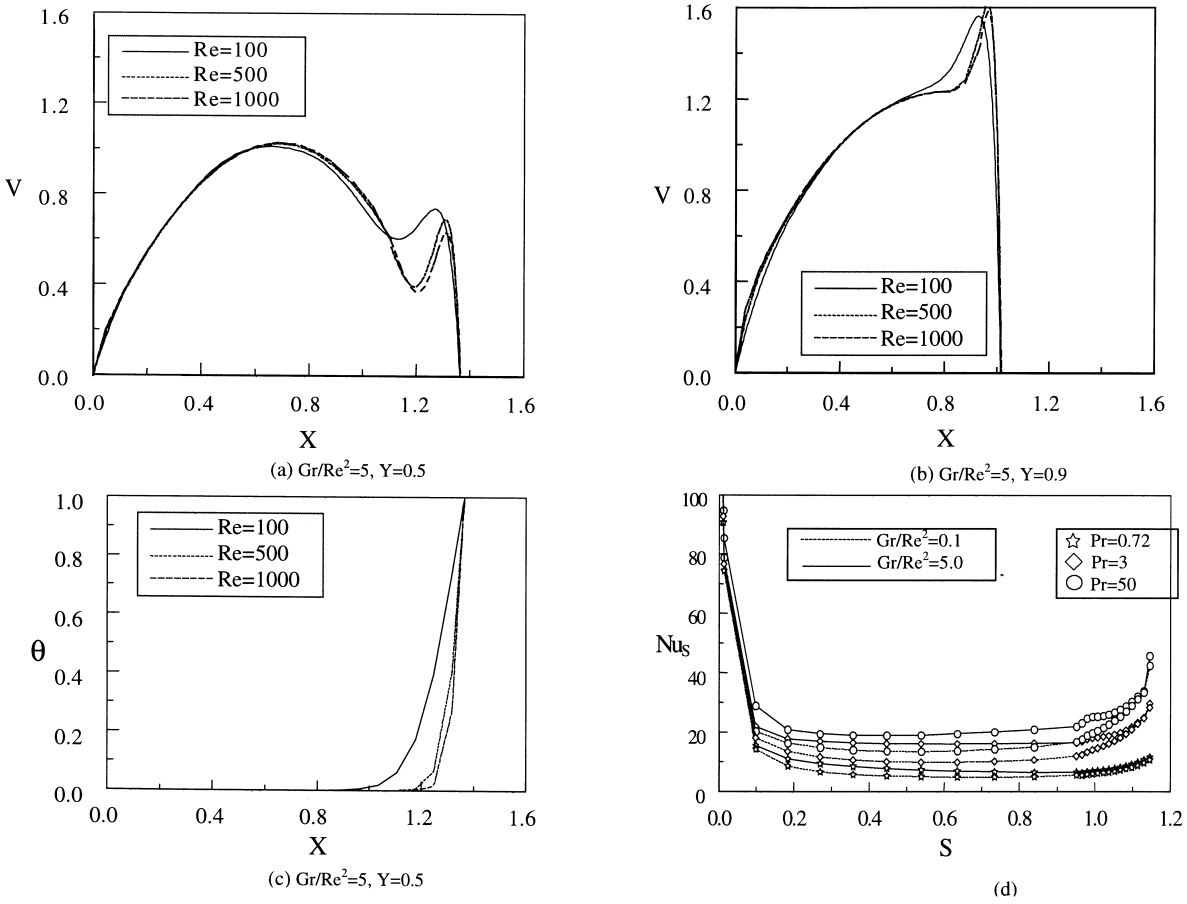

Fig. 7. (a)–(b) Velocity, (c) temperature, and (d) Nusselt number distribution for different values of Re (concave entry; $R/L = 1.25$, $Pr = 0.72$).

area further increases the velocity and enhances the forced convection contribution to total heat transfer. This produces a corresponding increase in Nu_S near the channel exit.

The overall heat transfer results ($\overline{Nu}$) displayed in Table 2 show $\overline{Nu}$ values in the concave-entry channel to increase with Re as expected, and they are generally higher than the corresponding values in the convex-entry channel. The $\overline{Nu}$ values decrease with increasing R/L, but are always greater than the case of a straight channel of equal height. However, when compared with a straight vertical channel of equal heated surface area, at a given Re, there is a critical Gr/Re^2 below which heat transfer enhancement is obtained with concave-entry channels. At $R/L = 1.04$, the degradation window where enhancement is not obtained is small, and is limited to $Re \leq 200$, and $Gr/Re^2 \geq 1$ for $Re = 100$ and $Gr/Re^2 \geq 3$ for $Re = 200$. As R/L increases, so does the degradation window, and at $R/L = 2.5$, no enhancement is obtained only for $Gr/Re^2 \geq 3$ at any Re.

6.2. Effects of Prandtl number

6.2.1. Velocity and temperature distributions

The effects of Pr on the velocity profiles across the channel mid-height are shown in Fig. 8(a) and (b) for $Gr/Re^2 = 0.1$ and 5, respectively. The temperature distribution corresponding to Fig. 8(a) is shown in Fig. 8(c). The behavior shown in Fig. 8(a)–(c) is quite similar to that shown in Fig. 6(a)–(c), and the reasons for these variations are quite similar to that noted previously. As depicted, increasing Pr has almost no effect on the general shape of the velocity distribution at low values of Gr/Re^2. On the other hand, Pr is seen to greatly affect the velocity profiles at higher values of Gr/Re^2. This is because, as stated earlier, Gr/Re^2 controls the coupling between the energy and the flow equations, and Pr, which appears in the energy

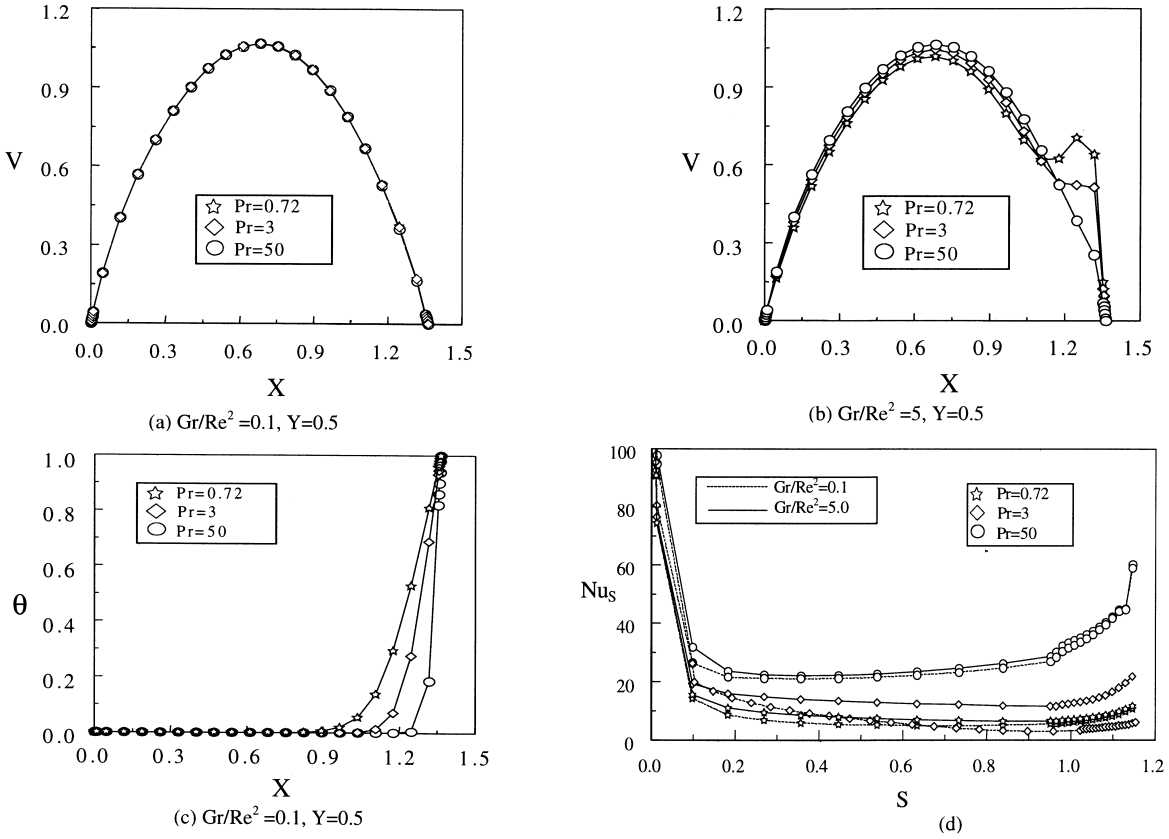

Fig. 8. (a)–(b) Velocity, (c) temperature, and (d) Nusselt number distribution for different values of Pr (concave entry; $R/L = 1.25$, $Re = 100$).

equation has an important effect only when this coupling is strong.

6.2.2. Nusselt numbers

The effects of varying Pr on local Nusselt number variation along the hot wall are illustrated in Fig. 8(d) ($Re = 100$). In general, due to higher temperature gradients associated with higher values of Pr, the level of Nu_S increases as Pr increases. Moreover, results presented in Fig. 8(d) suggest the presence of a critical Pr for which natural convection effects are maximized. Furthermore, as the flow approaches the exit, Nu_S increases significantly due to flow acceleration induced by the decrease in the channel cross-section.

The average Nusselt number values presented in Table 3 indicate higher heat transfer rates in concave-entry channels over a straight channel of equal height at all values of Pr. The enhancement levels increase with increasing Pr. Compared to the effect of Pr, the effect of Gr/Re^2 is more modest. For example, at $Pr = 0.72$, the enhancement decreases from 14.3% at $Gr/Re^2 = 0$ to 12.7% at $Gr/Re^2 = 5$, while for $Pr = 50$, the enhancement increases from 43.2% at $Gr/Re^2 = 0$ to 44.8% at $Gr/Re^2 = 5$. This indicates a dominance of forced convection effects in concave-entry channels. Moreover, Table 3 indicates the presence of a critical Gr/Re^2 value below which heat transfer in concave-entry channels is higher than its counterpart in straight channels of equal heated surface area. This critical value increases with Pr and decreases with R/L.

6.3. Average Nusselt number correlation

The average Nusselt number over the heated surface is correlated, as before, by Eq. (6), with the CE function representing the effects of concave rather than the convex entry. The CE functional expression for the concave entry case is correlated by:

$$\mathrm{CE} = 0.8F_5\left[\left(\frac{R}{L}\right)^*\right] \times Re^{0.05} \times Pr^{0.02} \times \left(\frac{Gr}{Re^2}+1\right)^{-0.015} \tag{12}$$

where

$$F_5\left[\left(\frac{R}{L}\right)^*\right] = \left[\left(\frac{R}{L}\right)^*\right]^{0.1} \times \left\{135 - 59\left(\frac{R}{L}\right)^* + 24.5\left[\left(\frac{R}{L}\right)^*\right]^2\right\} \tag{13}$$

The above correlation is again accurate to within 15%.

7. Closing remarks

The effects of Re and Pr on mixed laminar convection heat transfer in convex- and concave-entry channels are studied numerically. A detailed investigation has been undertaken for different values of Re, Pr, Gr/Re^2 and R/L. Comparisons have been made with equivalent straight channel configurations. The following are some of the important observations made:

Convex-entry channel

1. For $R/L = 1.04$ and 1.25, flow separation is observed along the convex heated surface at low Gr/Re^2 due to adverse pressure gradient effects associated with increasing cross-sectional area in the flow direction. As Gr/Re^2 increases to 5, buoyancy induced acceleration is sufficient to eliminate this separation at $Re = 100$ and 500, while at $Re > 500$, the large separation reduces to a small lifted vortex. The buoyancy-induced acceleration near the heated curved wall produces a velocity-peak in the boundary layer adjacent to the heated surface and is associated with corresponding deceleration away from the wall which then leads to flow separation on the opposite wall. At high Pr ($=50$) however, no flow separation on the opposite wall is obtained. For $R/L = 2.5$, the adverse pressure gradient is not sufficiently strong to cause flow separation along the heated wall.
2. For low Gr/Re^2, the Nusselt number reaches a minimum near the onset of flow separation along the heated wall of the convex-entry channel, and then increases toward the channel exit. This behavior is accentuated at high Pr. For high Gr/Re^2, since no flow separation exists along the heated wall, the behavior is more monotonic.
3. The effect of increasing Prandtl number on the total heat transfer is considerably greater than the effect of increasing Gr/Re^2. The overall heat transfer in the convex-entry channel is greater than the overall heat transfer in a straight channel of equal height only for low R/L, high Gr/Re^2 and high Pr values. The comparison is not favorable when the convex-entry channel is compared with a vertical channel of equal heated length or area.

Concave-entry channels

4. For concave-entry channels, flow separation is not encountered. The decreasing cross-sectional area combined with buoyancy increase the channel velocities and the near wall gradients. Therefore, surface heat transfer rates are considerably greater than in a convex-entry channel.

5. The near wall flow acceleration due to buoyancy is most pronounced for low Prandtl number in the concave-entry channel, and is the smallest at high Prandtl numbers. The near wall flow acceleration leads to the Nusselt number increasing toward the concave-entry channel exit following a minimum in the mid-regions of the channel.
6. The overall heat transfer in a concave-entry channel is always greater than a straight channel of equal height. When compared to a straight channel of equal heated surface area, there is a critical Gr/Re^2 value, below which heat transfer enhancement is obtained with concave-entry channels.

Acknowledgements

The financial support provided by the University Research Board of the American University of Beirut through grant No. 113040-48756 is gratefully acknowledged.

References

[1] F. Moukalled, A. Doughan, S. Acharya, Mixed convection heat transfer in concave and convex channels, in: P.H. Oosthuizen, T.S. Chen, S. Acharya, B.F. Armaly, D.W. Pepper (Eds.), ASME National Heat Transfer Conference, Baltimore, ASME-HTD, vol. 346, 1997.
[2] Ostrach, S. Combined natural and forced convection laminar flow and heat transfer of fluids with and without heat source in channels with linearly varying wall temperature. NACA TN 3141, 1954.
[3] W. Aung, G. Worku, Developing flow and flow reversal in a vertical channel with asymmetric wall temperatures, J. Heat Transfer 108 (1986) 299–304.
[4] W. Aung, G. Worku, Mixed convection in ducts with asymmetric wall heat fluxes, J. Heat Transfer 109 (1987) 947–951.
[5] E. Naito, Y. Nagano, Combined forced and free upward-flow convection in the entrance region between inclined parallel plates, J. Heat Transfer 111 (1989) 675–682.
[6] L.N. Tao, On combined free and forced convection in channels, J. Heat Transfer 82 (1960) 233–238.
[7] W.T. Lawrence, J.C. Chato, Heat transfer effects on the developing laminar flow inside vertical tube, J. Heat Transfer 88 (1966) 214–222.
[8] S. Habchi, S. Acharya, Laminar mixed convection in a symmetrically or asymmetrically heated vertical channel, Numerical Heat Transfer 9 (1986) 605–616.
[9] W. Aung, An experimental study of laminar heat transfer downstream of backsteps, J. Heat Transfer 105 (1983) 823–829.
[10] J.C. Vogel, J.K. Eaton, Combined heat transfer and fluid dynamic measurements downstream of a backward facing step, J. Heat Transfer 107 (1985) 922–929.
[11] S. Acharaya, S. Habchi, Laminar mixed convection in a partially blocked, vertical channel, Int. J. Heat Mass Transfer 29 (1986) 1711–1722.
[12] H.I. Abu-Mulaweh, B.F. Aramaly, T.S. Chen, Effects of upstream wall heating on mixed convection in spearated flows, J. Thermophysics and Heat Transfer 9 (1995) 715–721.
[13] H.I. Abu-Mulaweh, B.F. Aramaly, T.S. Chen, Measurements in buoyancy-opposing laminar flow over a vertical backward-facing step, J. Heat Transfer 116 (1994) 247–250.
[14] B. Hong, B.F. Armaly, T.S. Chen, Laminar mixed convection in a duct with a backward-facing step: the effects of inclination angle and Prandtl number, Int. J. Heat and Mass Transfer 36 (1993) 3059–3067.
[15] M.D. Kestoras, T.W. Simon, Hydrodynamic and thermal measurements in a turbulent boundary layer recovering from a concave curvature, J. Turbomachinery 114 (1992) 891–898.
[16] M.V. Finnis, A. Brown, The streamwise development of gortler vortices in a favorable pressure gradient, J. Turbomachinery 118 (1996) 162–171.
[17] F. Moukalled, A. Doughan, S. Acharya, Mixed convection heat transfer in concave and convex channels, in: P.H. Oosthuizen, T.S. Chen, S. Acharya, B.F. Armaly, D.W. Pepper (Eds.), ASME National Heat Transfer Conference, Baltimore, August, HTD-346, vol. 8, 1997.
[18] S.V. Patankar, Numerical Heat Transfer and Fluid Flow, Hemisphere, New York, 1980.
[19] S.V. Patankar, D.B. Spalding, A calculation procedure for heat, mass and momentum transfer in three-dimensional parabolic flows, Int. J. Heat Mass Transfer 15 (1972) 1787–1795.
[20] Peric, M. A finite volume method for the prediction of three-dimensional fluid flow in complex ducts, PhD thesis, Imperial College of Science and Technology, University of London, 1985.
[21] J.F. Thompson, Numerical Grid Generation, North-Holland, Amsterdam, 1982.
[22] T.S. Chen, B.F. Armaly, N. Ramachandran, Correlation for laminar mixed convection flows on vertical, inclined, and horizontal flat plates, J. Heat Transfer 108 (1986) 835–840.